Physics of Fluids

Sessile liquid drops damp vibrating structures

Cite as: Phys. Fluids **33**, 062113 (2021); https://doi.org/10.1063/5.0055382
Submitted: 28 April 2021 . Accepted: 27 May 2021 . Published Online: 15 June 2021

MD Erfanul Alam, and Andrew K. Dickerson

Physics of Fluids ARTICLE scitation.org/journal/phf

Sessile liquid drops damp vibrating structures

Cite as: Phys. Fluids **33**, 062113 (2021); doi: 10.1063/5.0055382
Submitted: 28 April 2021 · Accepted: 27 May 2021 ·
Published Online: 15 June 2021

View Online Export Citation CrossMark

MD Erfanul Alam and Andrew K. Dickerson[a]

AFFILIATIONS

Department of Mechanical and Aerospace Engineering, University of Central Florida, Orlando, Florida 32816, USA

[a]Author to whom correspondence should be addressed: dickerson@ucf.edu

ABSTRACT

In this study, we explore the vibration damping characteristics of singular liquid drops of varying viscosity and surface tension resting on a millimetric cantilever. Cantilevers are displaced 0.6 mm at their free end, 6% their length, and allowed to vibrate freely. Such ringdown vibration causes drops to deform, or slosh, which dissipates kinetic energy via viscous dissipation within the drop and through contact line friction. Damping by drop sloshing is dependent on viscosity, surface tension, drop size, and drop location. A solid weight with the same mass as experimental drops is used to compare against the damping imposed by liquids, thereby accounting for other damping sources. Neither the most viscous nor least viscous drops studied imposed the greatest damping on cantilever motion. Instead, drops of intermediate viscosity strike the most effective balance of sloshing and internal dissipative capacity. Very thin cantilevers with sloshing drops express more than one dominant frequency and vibrate erratically, often shifting phase, presenting a challenge for quantification of damping. Finally, we introduce a new dimensionless group aimed at incorporating all salient variables of our cantilever-drop system.

I. INTRODUCTION

Simple cantilever motion is generally well-understood and numerous models are available to determine both aerodynamic damping[1–3] and internal dissipation.[4–6] Dissipative forces arise from the cantilever material and external forces such as air drag and decaying free vibration.[7] Mass placed at the cantilever tip is a straightforward means to augment cantilever dynamics compared to naked cantilevers, including the nature of vibration damping. Rigid masses contribute no appreciable internal damping, but impart inertia that can prolong vibration. In contrast, particle impact dampers[8–10] (PIDs) hold hundreds to thousands of particles as a single concentrated mass that moves freely within a rigid shell to produce damping via particle impact,[9–14] friction,[15–18] and hysteretic particle deformation.[17,18] PIDs are effective over wide temperature and frequency ranges and can be found in applications including tennis rackets,[19] spacecraft,[20] turbomachinary,[21] and civil structures.[22]

Analogous to the impact of particles in a PID, liquid motion at all scales, both continuous flow and oscillatory motion, dissipates energy. Liquid sloshing in open containers with external excitation is an important phenomenon in engineering applications including trucking liquids,[25–27] fuel sloshing and buffeting problems of aircraft,[26,27] and creation of acoustic noise in automotive fuel tanks.[30–32] Both theoretical[33–35] and experimental[34,35] analyses have been extensively employed to examine the physics of liquid motion damping by sloshing in a container by tracking the motion of the free surface. Energy dissipation is likewise pertinent for exceedingly small liquid bodies and singular drops. Inertial forces deform liquid drops while surface tension imparts sphericalness to gas–liquid interfaces. When a drop is deformed from equilibrium, its return to equilibrium is achieved by performing damped oscillations[38–42] or sloshing. The capability of drops to damp disturbances across ranges in size, viscosity, and surface tension remains understudied.

Millimetric cantilevers provide a simple dynamic system to investigate damping by liquid drops, and such a system is schematized in Fig. 1(a). Below critical accelerations, drops remain atop the cantilever and slosh, rather than eject, as the cantilever vibrates. At the scale where drops are large enough to deform under imposed acceleration and small enough to remain a single entity, they behave similar to miniature PIDs by contributing a mass, which deforms with cantilever motion[38,41,42] as pictured in Fig. 1(b). A qualitative visual of drop damping compared to a solid mass of equivalent weight can be seen by plotting vibration amplitude y vs time t in Fig. 1(c). Surface tension constrains drop flow while governing an equilibrium shape. Viscosity acts in concert to further restrain flow and dissipate energy. Damping by a sloshing drop has been quantified for very narrow conditions when the cantilever base is excited in first-mode vibration.[38,43] Damping by drops is known to depend on base frequency, cantilever surface wettability, drop position, drop size, and liquid viscosity.[38,43] With a fixed cantilever base, free vibration is induced by an initial deflection of the free end. In this study, we consider the damping

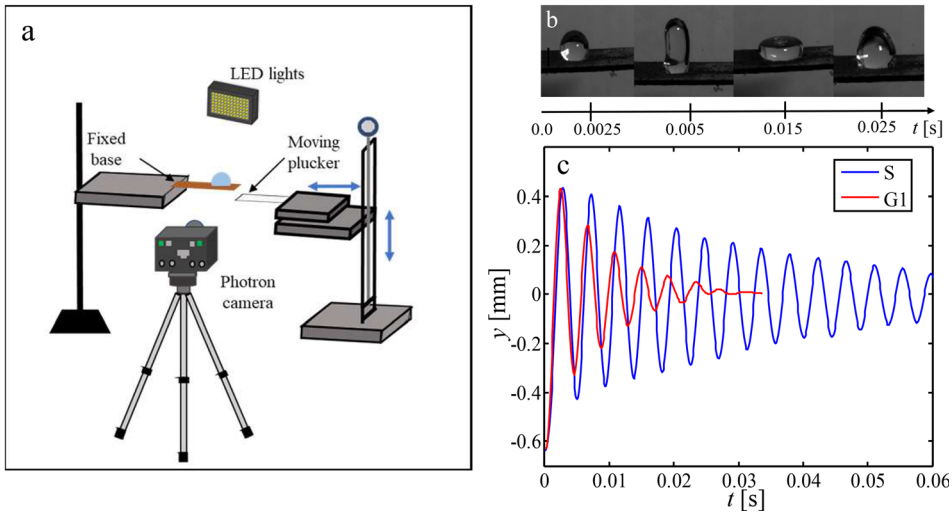

FIG. 1. (a) Experimental setup of vibrating cantilever using moving plucker produces the initial tip deflection. (b) Photo sequence of drop deformation for glycerin (G1). (c) Comparison of cantilever tip displacement with solid (S) and liquid (G1) masses.

ringdown vibration of a fixed, $10 \times 3.6\text{-mm}^2$ cantilever by a sessile drop placed at a fixed location on the dorsal surface of the cantilever. Initial tip deflection is applied so the ensuing inertial force does not overcome liquid–solid adhesion to eject the drop. Newtonian test drops vary in composition to obtain contrasting viscosity and a range of surface tension. We present our experimental methods in Sec. II, theoretical considerations in Sec. III, and results in Sec. IV. A discussion of results follows in Sec. V.

II. METHODS

We construct cantilevers from Kapton polymide film, elastic modulus $E = 2.5$ GPa, of length $\ell = 10$ mm (0.002 in.), and width 3.60 mm (0.14 in.), sourced from McMaster-Carr. Cantilevers are cut to size with a GlowForge laser cutter at sufficient power to make a cut while not charring and beveling edges. We use three different thicknesses of Kapton, which are $t_h = 2$-mil (0.051 mm), 5-mil (0.127 mm), and 10-mil (0.254 mm), and prepare cantilevers of mass $m_c = 2.2$, 5.5, and 11.7 mg, respectively. Cantilevers are attached to a fixed post with cyanoacrylate while a plucker produces the initial tip deflection. The plucker is a razor blade afixed to a micromanipulator. Trials in which cantilevers release from the plucker prematurely are disregarded. A schematic of our experimental setup is shown in Fig. 1(*a*). NeverWet® hydrophobic coating is used to increase the equilibrium contact angle to $\theta_c = 129 \pm 9.57°$, N = 87. It should be noted that different liquids express different contact angles. Greater values of θ_c are achievable by multiple applications of NeverWet, but superfluous hydrophobicity enables drop relocation.[38,43] Drops of mass $m_d = 2.0 \pm 0.1$ mg, N = 87 are placed atop the cantilever by hand using a syringe at a distance of $x_0 = 6.89 \pm 0.32$ mm, N = 87 from the fixed end. The trial-and-error ensures drop size matches the desired mass, within 10%. The target drop radius is determined from formulas presented in the supplementary material and Fig. S1. The drop location was chosen such that drops rest near the cantilever tip without spilling over the tip when deformed. Liquid drop properties are augmented by mixing imitation honey (H), glycerin (G), and water (W) to various ratios by volume. With satisfactory drop size and placement, each condition has three replicates. Our naming scheme for liquid mixtures dictates the number of parts following the liquid abbreviation. For example, "G3W1" denotes the mixture is composed of three parts glycerin and one part water by volume. We change the liquid surface tension by adding a very small amount of dish soap to the mixture. Surface tension of the mixtures is measured with a SITA DynoTester$^+$ surface tensiometer using the bubble pressure method, and visocity of the mixtures is measured using a Brookfield DV-II Pro Viscometer. The viscosity and surface tension of our test liquids are given in Table I.

Drop sloshing events and cantilever tip displacement are filmed with a Photron high-speed camera at 8100–8500 fps fitted with a Nikon Sigma APO Macro 150-mm f/2.8 lens. The scene is illuminated by GS Vitec MultiLED lights. Drop measurements, location, and cantilever motion are gathered with Open Source Physics Tracker and MATLAB. A Savitzky Golay filter with a third order polynomial and a span of 11 is used to remove artifacts from displacement and velocity curves.[45] Suitable filter parameters are chosen, which produces minimum deviation from the original experimental data.[48–51]

III. THEORETICAL CONSIDERATIONS

A. Quantifying damping capacity

Generally, damped systems in free vibration with unchanging mass can be described by a familiar equation of motion,

$$m\ddot{y} + c\dot{y} + ky = 0. \tag{1}$$

In our system, y is vertical tip displacement, mass $m = m_c + m_d$ and is nonuniformly distributed along the cantilever, the damping coefficient c is not constant, and the spring constant k is dependent on the cantilever material and thickness. The nonlinear behavior of damping, exacerbated by drop deformation across vibration cycles, is dependent on the vibration amplitude and necessitates the use of a simple analytical tool. We thus employ the specific damping capacity ψ, defined as

$$\psi = \frac{\Delta T}{T}, \tag{2}$$

where ΔT is the kinetic energy converted into heat or potential energy during one cycle and

TABLE I. Density, viscosity, and surface tension of different liquid mixtures.

Mixture	Symbol	Density, ρ (g/ml)	Viscosity, μ (cP)	Surface tension, σ (mN/m)	Ohnesorge number, Oh
H1	◯	1.39 ± 0.02	10 000	310[a]	17.06
H3G1	△	1.25 ± 0.02	3378 ± 6	100.2 ± 1.4	9.5
H1G1	▽	1.20 ± 0.01	1207 ± 5	97.4 ± 0.4	3.7
H1G3	∗	1.21 ± 0.01	975.4 ± 3.3	92.6 ± 0.5	2.9
G1	◇	1.21 ± 0.01	520.7 ± 3.4	83.7 ± 1.6	1.76
G3W1	□	1.19 ± 0.02	32.8 ± 1.3	78.9 ± 1.4	0.12
G1W1	•	1.10 ± 0.01	9.26 ± 1.12	75.6 ± 0.7	0.036
G1W3	◁	1.06 ± 0.01	3.14 ± 0.35	73.2 ± 1.5	0.013
W1	▷	0.983 ± 0.004	0.981 ± 0.007	71.7 ± 0.6	0.004

[a]From Ref. [46].

$$T = V^2\left[\frac{m_c}{6} + \frac{m_d}{2}\left(\frac{x_0}{\ell}\right)^2\right], \tag{3}$$

is the maximum kinetic energy of the cantilever during the cycle and V is the velocity of the cantilever tip. The energy dissipated during the ith cycle can be expressed as

$$\Delta T_i = T_i - T_{i+1} = (V_i^2 - V_{i+1}^2)\left[\frac{m_c}{6} + \frac{m_d}{2}\left(\frac{x_0}{\ell}\right)^2\right], \tag{4}$$

where specific damping capacity during the ith cycle is expressed as

$$\psi_i = \frac{V_i^2 - V_{i+1}^2}{V_i^2}, \tag{5}$$

with V measured at $y = 0$. In order to compare the response of cantilevers of varying stiffness, we introduce another dimensionless parameter, effective acceleration[12] Γ, as

$$\Gamma = \frac{A\omega^2}{g}, \tag{6}$$

where A, ω, and g are the amplitude, vibration frequency of the cantilever motion, and gravitational acceleration, respectively.

B. Energy dissipation due to viscosity

We employ an energy balance[50,51] on the cantilever at time $t = 0$ and after the end of the first cycle ($'$) to provide an additional method to quantify of energy dissipation due to drop sloshing,

$$E_\mu = \Delta E_p + \Delta E_s - E_d, \tag{7}$$

where E_μ includes energy dissipated internally by viscosity and by friction at the contact line.[54–56] The energy dissipated via aerodynamic and internal damping E_d is measured by using a solid mass, which cannot deform. The change in the cantilever's potential bending energy is

$$\Delta E_p = \frac{3EI}{2\ell^3}\left(y^2 - y'^2\right). \tag{8}$$

The deflection of the cantilever at release y is greater than the deflection after one cycle, y'. A change in the surface energy of the liquid drop can be measured by considering the change in the liquid–gas interface area and liquid–solid contact area,

$$\Delta E_s = \sigma\left(A_s - A_s'\right) + \pi\sigma\left(r_c^2\cos\theta_c - r_c'^2\cos\theta_c'\right), \tag{9}$$

where A_s and A_s', r_c and r_c', θ_c and θ_c' are the surface areas, contact radii, and contact angles of the liquid at $t = 0$ and after one cycle, respectively. Gravitation potential energy $\Delta E_g = m_c g(y_c - y_c') + m_d g(y_d - y_d')$, where y_c and y_d are the vertical positions of the cantilever's center of mass and cantilever surface beneath the drop, respectively, is omitted from Eq. (7) because we find ΔE_g to be one to three orders of magnitude less than the other energies of Eq. (7).

IV. RESULTS

A. Effect of surface tension on damping

We first examine the influence of sloshing liquid surface tension σ on the specific damping capacity ψ by fixing drop viscosity and using G3W1 modified with a surfactant. The severity of surface tension on changes ψ is highly dependent on cantilever flexibility. For our stiffest cantilever, with thickness 10-mil, there is no discernible influence on ψ to changes in surface tension across the cantilever's range of effective acceleration Γ as shown in Fig. 2(a). As expected, lower surface tension values promote greater drop deformation as seen by the image sequences in Figs. 2(c) and 2(d). We quantify the degree to which a drop deforms from its static state by measuring the flatness factor[42]

$$\delta^* = \frac{h}{d}\frac{d_0}{h_0}, \tag{10}$$

where h is the distance from the drop peak to substrate and d is the diameter of the drop contact patch. The static system expresses h_0 and d_0 dimensions, which are labeled graphically in Fig. 2(d). Moving contact lines ensures that the drop contact patch oscillates in time. We plot δ^* vs time t in Fig. 2(b) for all tested G3W1 drops, with a value measured every video frame. The curves of Fig. 2(b) stand testament to the chaotic nature of drop deformation while sloshing on an elastic substrate. A fast Fourier transform (FFT) for the flatness factor is provided in Fig. S2 of the supplementary material. The repeatability of ψ values across multiple trials is shown by plotting ψ vs Γ for multiple

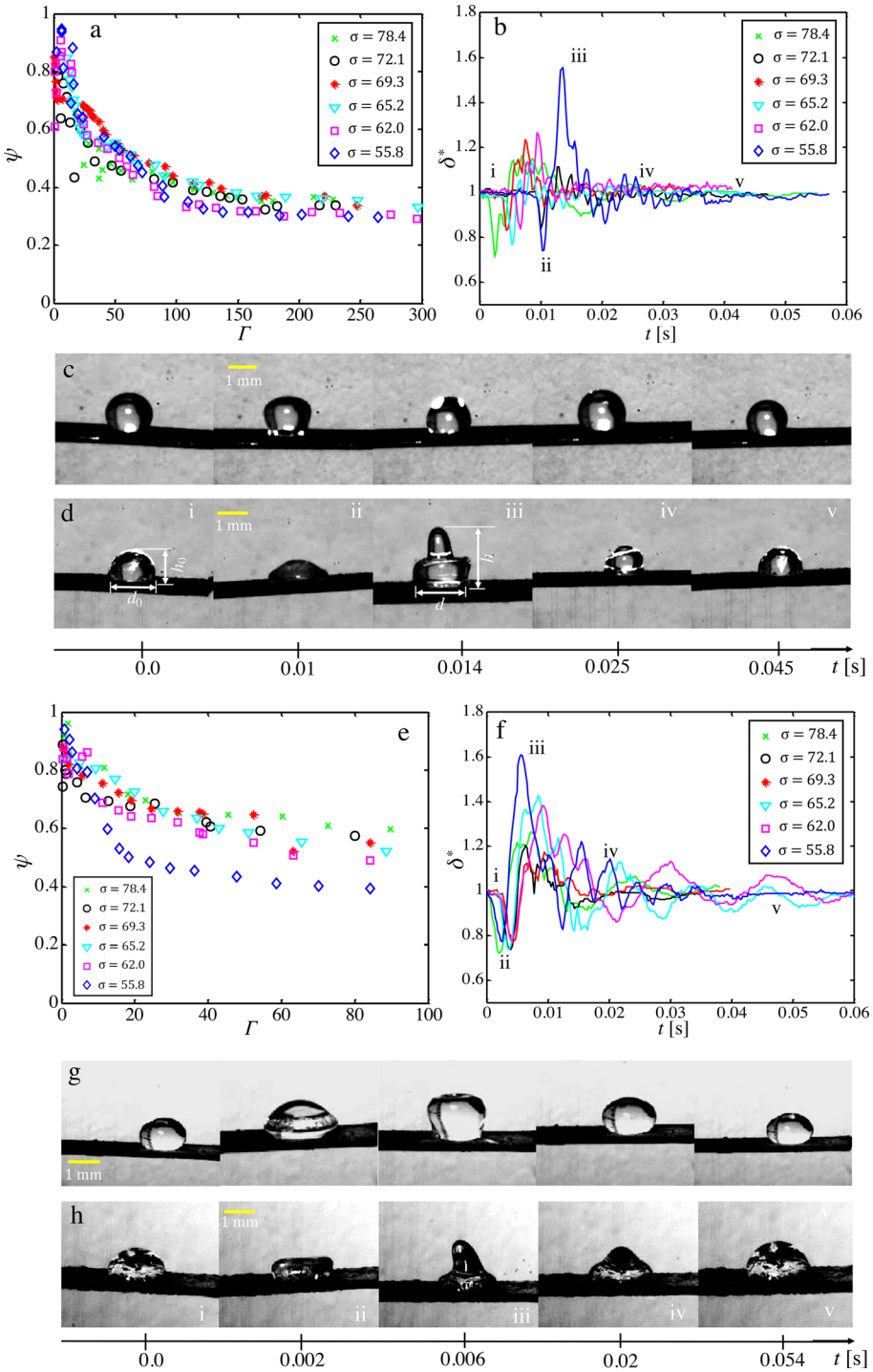

FIG. 2. The effect of surface tension on damping. (a) and (e) Specific damping capacity ψ vs effective acceleration Γ. (b) and (f) Temporal variation of flatness factor. (c), (d), (g), and (h) Photo sequences of drop sloshing for a G3W1 drop with surface tension value $\sigma = 78.4$ mN/m and $\sigma = 55.8$ mN/m, respectively. Panels (a)–(d) correspond to a 10-mil thick cantilever and panels (e)–(f) to a 5-mil cantilever. Values in the plots legends have units mN/m.

replicates in Fig. S3. We find replicate curves indistinguishable from one another for three representative surface tension values.

In contrast to a 10-mil cantilever, damping of the 5-mil cantilever by the liquid drop is generally enhanced by increasing surface tension in our range of experimental values as shown in Fig. 2(e). We visualize how σ affects damping by averaging the ψ values in Fig. 2(a) to produce $\bar{\psi}$. We plot $\bar{\psi}$ vs σ in Fig. 3 for both 10 and 5-mil cantilevers. One might expect that greater drop deformation [Fig. 2(f)] ensures

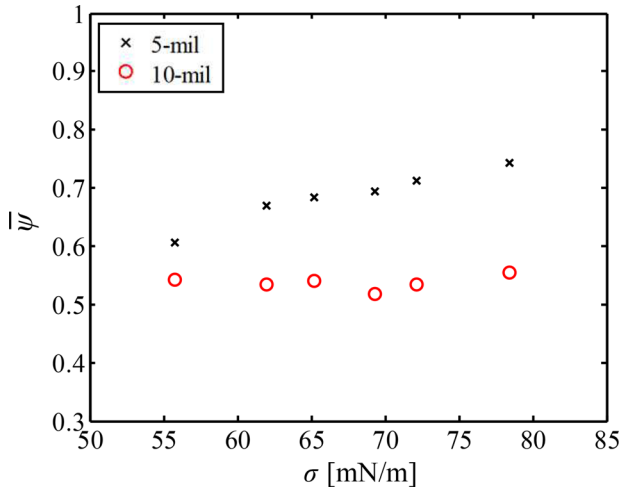

FIG. 3. Average damping capacity $\bar{\psi}$ vs G3W1 drop surface tension σ.

greater damping, but it should be noted that while lower surface tension drops are more easily deformed, they require less energy to do so; surface energy scales with surface tension.[51] Furthermore, greater surface tension values dictate that a greater volume of the static drop participates in deformation. In other words, greater surface tension allows the center of liquid mass to move further from the substrate as contact lines recede. The result is that internal energy dissipation by viscosity occurs within a larger fluid volume. A visual accompaniment of this argument is provided with images comparing the centroid of two G3W1 drops of different surface tension at their maximum δ^* in Fig. S4. The portion of the liquid drop pulled away from the substrate is greater for the higher surface tension liquid. Surface tension thus affects the mechanical impedance matching and force transmitted between the drop and cantilever. A quantitative description of internal dissipation for contrasting drop deformations is likely only feasible through simulation and outside the scope of this study. We discuss damping effects by drops of different viscosity in Sec. IV B.

The flexibility and diminutive inertia of the 2-mil cantilever permit the expression of higher-order behavior, which is surface tension dependent. We illustrate such behavior by the vibration curve in Fig. 4(a). Using a drop with $\sigma = 0.0784$ N/m, we witness that the sloshing drop can both amplify and suppress cantilever tip amplitude. When sloshing drops achieve a high δ^* value when the tip is at local minima, the drop suppresses the magnitude of the minima, as seen in the first trough of Fig. 4(a). A drop achieving a low δ^* value near local tip minima enhances the downward tip motion, as seen by the second trough of Fig. 4(a). We also find that the liquid drop is able to store elastic energy in its surface out-of-phase with cantilever motion, reducing the cantilever displacement to nearly zero for half a period [Fig. 4(a)]. A FFT of the vibration curve shown in Fig. 4(a) reveals two dominant vibration frequencies Fig. 4(b). Such higher-order behavior prevents the quantification of damping with Eq. (5) across the time of vibration. Reducing the surface tension of the drop reduces higher-order behavior but still reveals wave clipping at lower amplitudes. The cause for the shift in behavior with surface tension is unknown.

B. Effect of viscosity on damping

In Sec. IV A, we posit that surface tension modulates the volume of the drop participating in viscous damping. Viscosity, detached from surface tension, also governs deformation and energy dissipation. In this section, we compare the damping capacity of drops with a range of viscosity in order to identify an approximate optimum value. Neither an inviscid fluid nor a fluid of infinite viscosity, a solid, can damp vibration by viscosity, and thus some system-dependent intermediate value provides the greatest damping. The salient properties of test fluids are tabulated in Table I. Video compilations of each cantilever topped with each test liquid are available in Fig. 5 (Multimedia view). We choose test fluids in which we see a maximum damping capacity appear for neither the lowest nor highest viscosity and covering $0.89 - 10^3$ cP.

We plot specific damping capacity ψ vs effective acceleration Γ in Figs. 6(a)–6(c). As with surface tension, ψ is cantilever dependent. The stiffest 10-mil cantilever is damped most effectively by H1G3 (975 cP), as shown in Fig. 6(a). The intermediate 5-mil cantilever is damped best by the less viscous G3W1 (33 cP), as shown in Fig. 6(b). The thinnest 2-mil cantilever is damped best by the H1G3, as shown in Fig. 6(c), but we were unable to measure ψ across the entire vibration curve for G3W1, G1W1, G1W3, and W1 due to the higher-order behavior discussed above [Sec. IV A, Figs. 4 and 5(c) (Multimedia view)]. Temporal displacement curves for G1W3 and W1 are given in Fig. S5 of the supplementary material. For all three cantilevers, the most viscous liquid, H, has a similar specific damping curve to the solid mass as shown in Figs. 6(a)–6(c).

We acknowledge we cannot completely decouple changes in surface tension among the test fluids in Table I from variation in viscosity. Unification of viscosity and surface tension into a single dimensionless group can be done with the Ohnesorge number, $\mathrm{Oh} = \mu(\rho\sigma R)^{-1/2}$, where R is the static drop radius and μ is viscosity. It is noteworthy that an increase in viscosity of 1000× is accompanied by an increase in surface tension of 1.37×, so Oh values in our tests are driven primarily by changing viscosity. For the first vibration cycle, corresponding to the rightmost points in Figs. 6(a)–6(c), we plot ψ vs Oh in Fig. 7. For all cantilevers, we witness a rise in ψ from the lowest values of Oh, and a fall in ψ after $\mathrm{Oh} \approx 2.5$. While Fig. 7 does not reveal the critical Oh value that maximizes damping, we infer it lies in the range of $1 - 5$ for all cantilevers. The temporal plots of δ^* in Figs. 6(d) and 6(e) reveal the nature of drop deformation across viscosity, namely, that the two least viscous fluids undergo significant deformation compared to the rest. Thus, a trade-off between deformation and the ability of viscosity to dissipate energy emerges from Fig. 7, with the composition of this trade-off driven by cantilever dynamics. The relation between drop deformation, quantified with flatness factor δ^*, and viscosity is shown in Fig. 8. The heatmap of Fig. 8 reveals that intermediate levels of δ^* correspond to the greatest damping.

By calculating the energy lost to viscosity and contact line friction during the first vibration cycle, we can generate an alternative means to find the "sweet spot" in Oh with our cantilevers. Solving Eq. (7) with Eqs. (8) and (9) accounts for changes in cantilever potential bending energy (ΔE_p), the energy stored in the drop surface (ΔE_s), and a lumped energy dissipation present without drops (E_d). We plot E_μ normalized by the initial potential bending energy of a static cantilever $E_0 = 3EIy^2/2\ell^3$ in Figs. 8(d)–8(f). Peak viscous dissipation occurs at

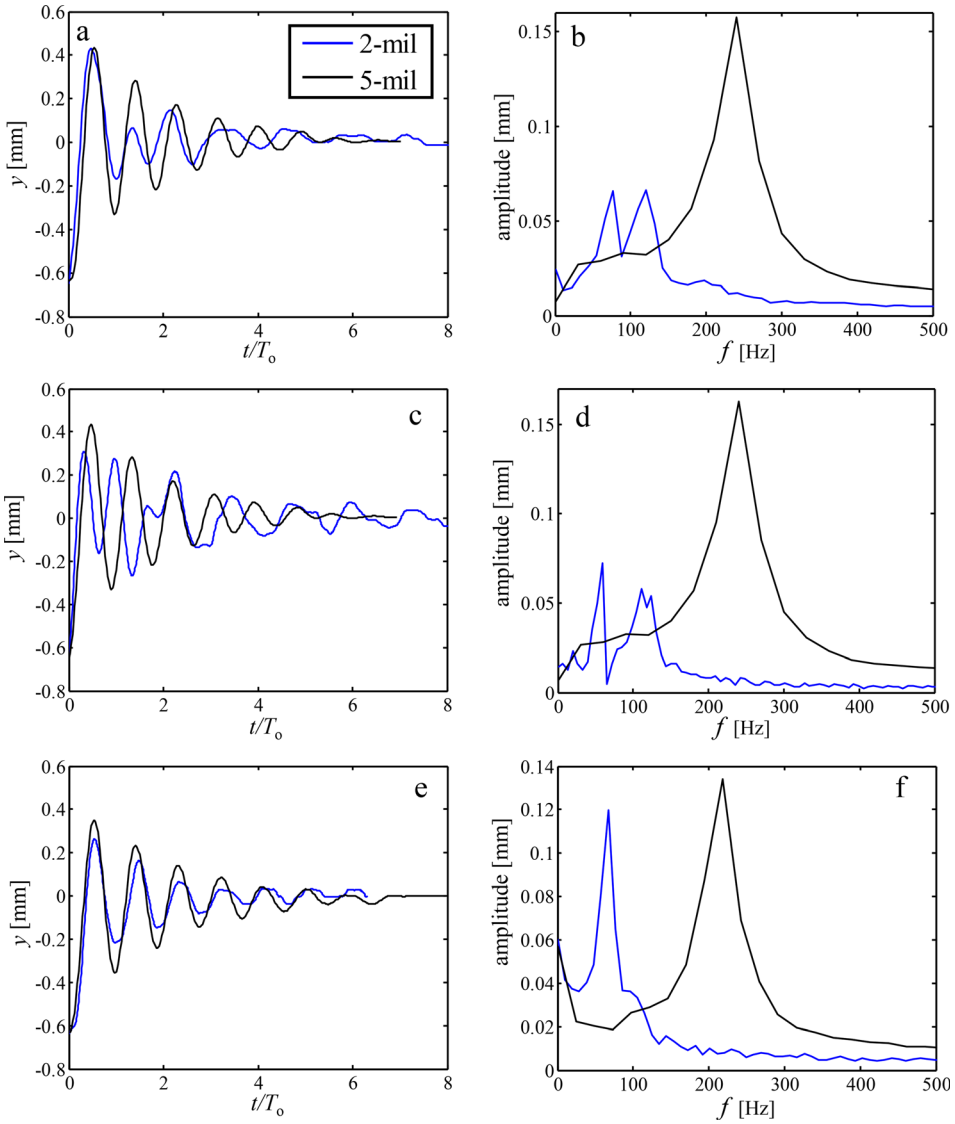

FIG. 4. Time response [(a), (c), and (e)] and frequency response [(b), (d), and (f)] with G3W1 drop ($\mu = 32.8$ cP) with surface tension $\sigma = 78.4$ mN/m [(a) and (b)], $\sigma = 69.3$ mN/m [(c) and (d)] and $\sigma = 55.8$ mN/m [(e) and (f)].

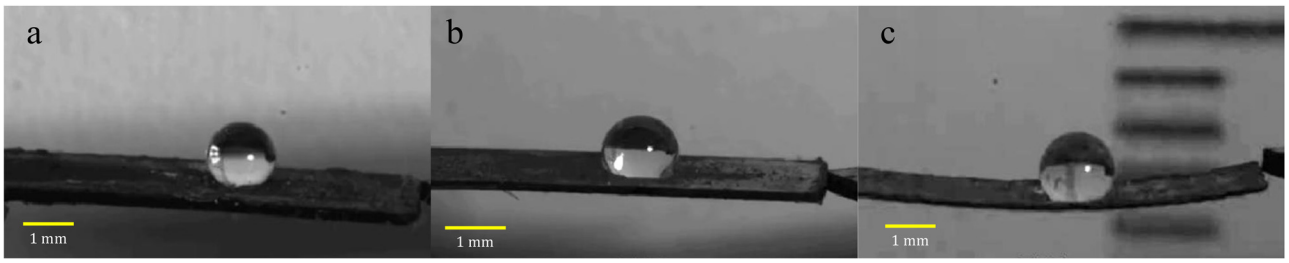

FIG. 5. Experimental video compilation of (a) 10-, (b) 5-, and (c) 2-mil thick cantilevers topped by the gamut of experimental liquid drops. Each video is slowed 270×. Multimedia views: (a) https://doi.org/10.1063/5.0055382.1, (b) https://doi.org/10.1063/5.0055382.2, (c) https://doi.org/10.1063/5.0055382.3

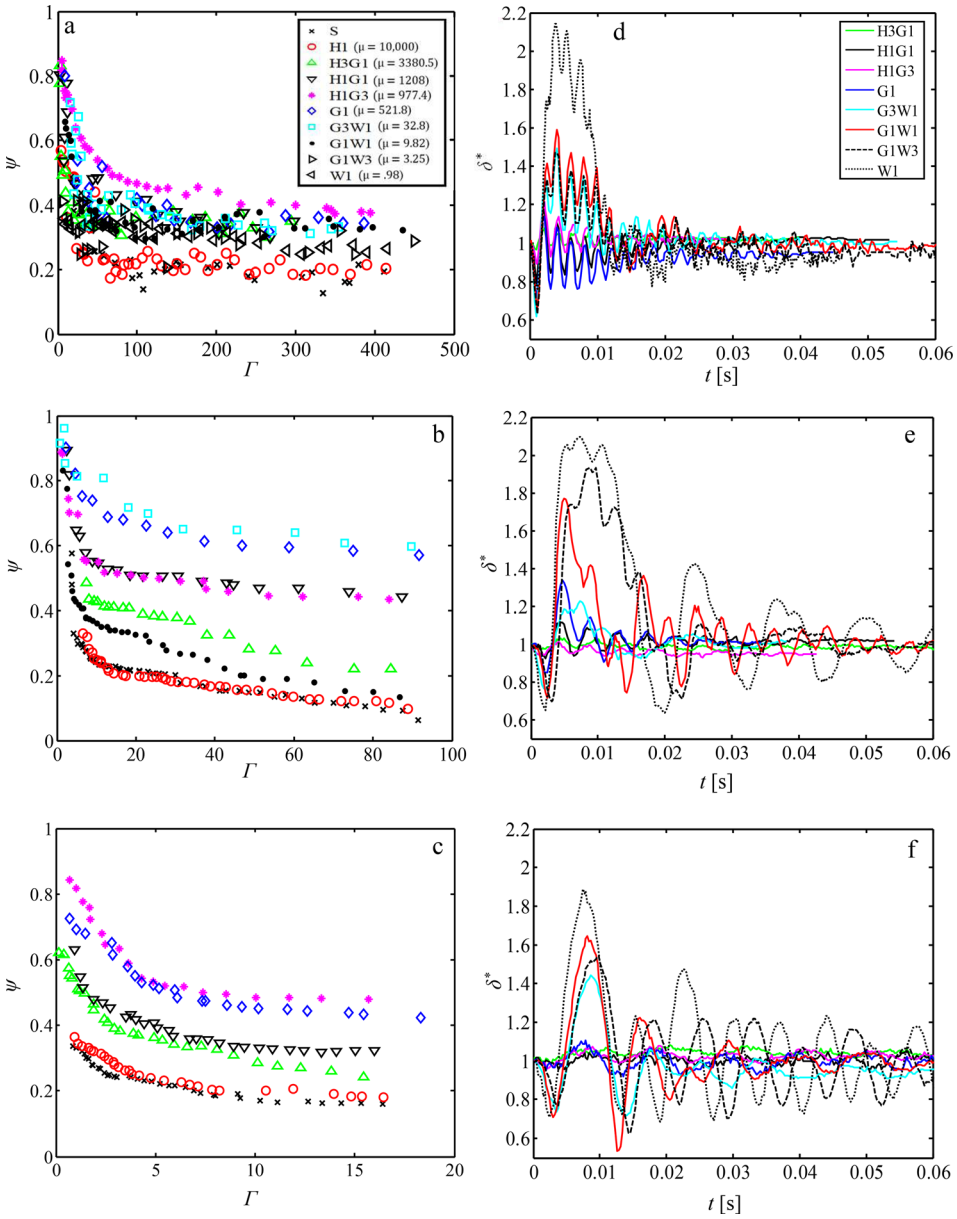

FIG. 6. Damping changes with viscosity. (a)–(c) Specific damping capacity ψ vs effective acceleration Γ. (d)–(f) Temporal variation of flatness factor. Each row represents a different cantilever: 10- [(a) and (d)], 5- [(b) and (e)], and 2-mil [(c) and (f)]. The legend in panel (a) applies to panels (a)–(c); viscosity values have units of cP. The legend in panel (d) applies to panels (d)–(f).

Oh $\approx 1 - 2.5$ for all cantilevers, also aligning with the greatest ψ values as expected.

C. Evaluating damping capacity in the frequency domain

A presentation of vibratory behavior modulation by drops would be incomplete without examining how drop properties influence frequency. As expected, stiffer cantilevers naturally vibrate at a higher frequency. We examine the effect of fluid viscosity on frequency modulation by nondimensionalizing damped natural frequency f by that measured for cantilevers with solid masses. This metric $f^* > 1$ for all experimental liquids is shown in Fig. 9(b). As viscosity rises and liquids behave more solid-like, $f^* \to 1$. We rationalize that decreasing viscosity allows for a virtual disconnection between the cantilever and drop's center of mass, much like relaxing a spring. Thus, from the viewpoint of frequency, low viscosity effectively reduces a drop's inertia. While viscosity inherently enhances energy dissipation, we again see that viscosity reduces the number of oscillations a drop can undergo in a given time. We are again reminded that there exists an intermediate viscosity, which optimizes damping.

Like many other problems in fluid mechanics, we seek a dimensionless group that permits the incorporation of salient system properties. The most appropriate, previously used dimensionless group

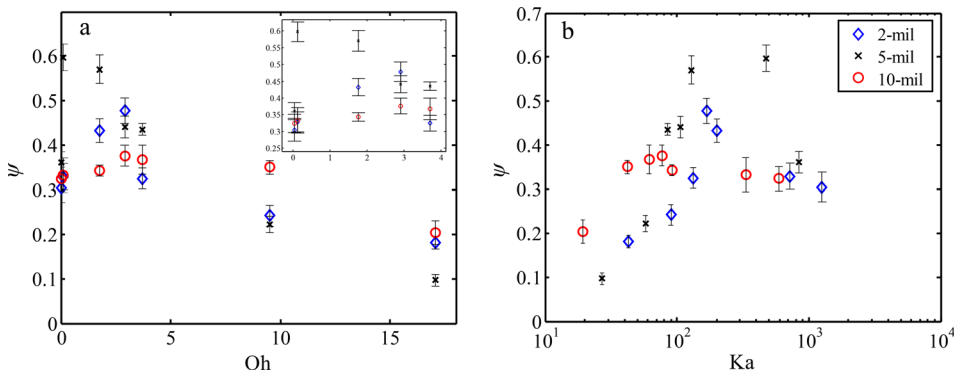

FIG. 7. Combined influence of viscosity and surface tension on damping. Specific damping capacity ψ vs Ohnesorge number (a) and Kauffman number (b). Error bars represent standard deviation in damping capacity.

includes fluid properties and frequency (to the author's knowledge) is the Womersley number[55] $\mathrm{Wo} = L(2\pi f \rho/\mu)^{\frac{1}{2}}$, traditionally used to describe unsteady internal flow with a length scale L representing that of a solid boundary such as diameter. The Womersley number is limiting in our case because it does not permit the incorporation of both cantilever and drop length scales. We thus pose a new group, which we dub the Kauffman number, after a previous collaborator instrumental in our first cantilever studies, Alam *et al.*,[38]

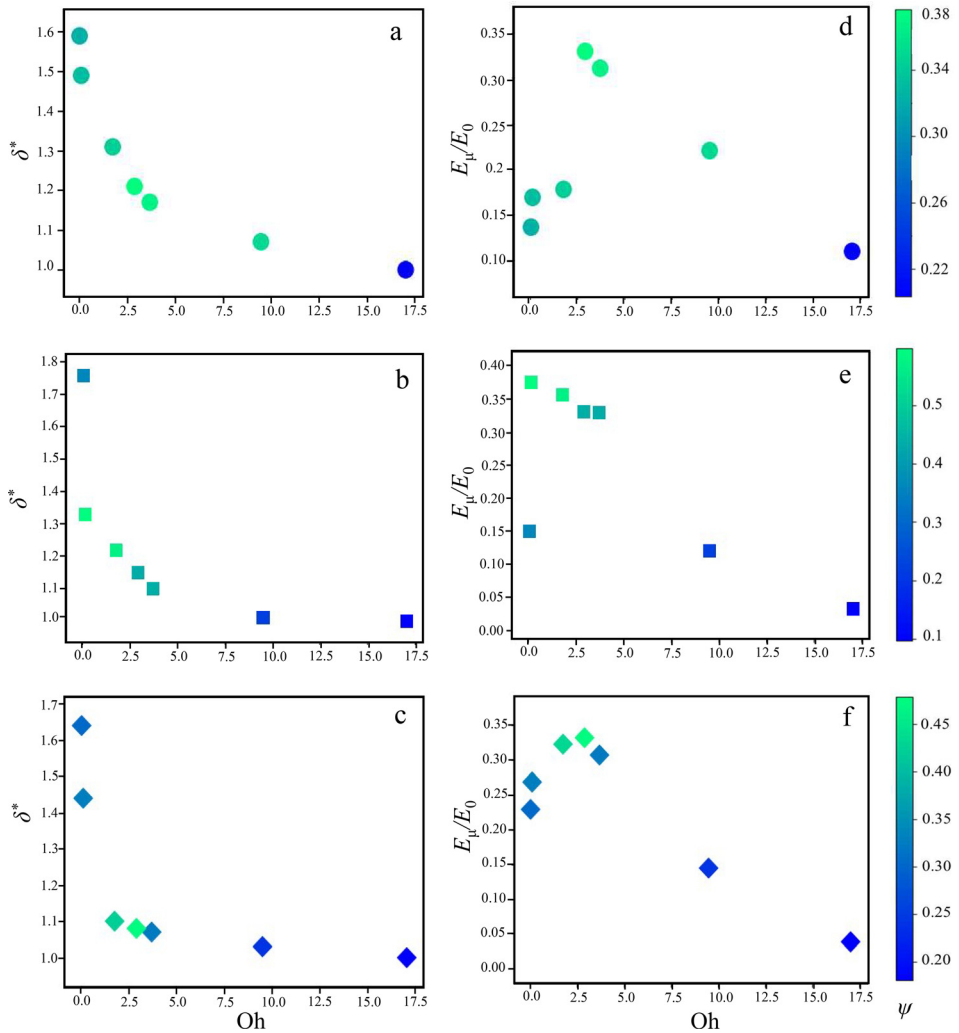

FIG. 8. Flatness factor δ^* (a)–(c) and nondimensionalized viscous energy dissipation E_μ/E_0 (d)–(f) vs Ohnesorge number. Each row represents a different cantilever: 10- [(a) and (d)], 5- [(b) and (e)] and 2-mil [(c) and (f)]. The color bar in each row applies to both panels in the row.

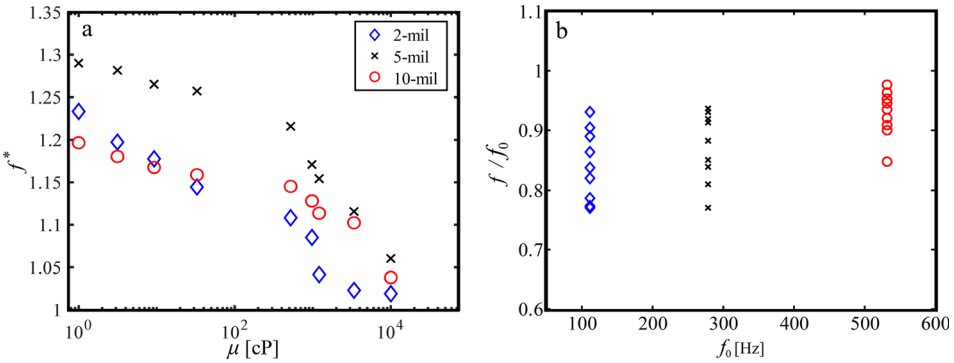

FIG. 9. (a) Normalized vibration frequency vs drop viscosity. (b) Vibration frequency normalized by vibration frequency without added mass (f/f_0) vs f_0. The legend in (a) corresponds to both panels.

$$\mathrm{Ka} = R\frac{\ell}{t_h}\left(\frac{2\pi f\rho}{\mu}\right)^{\frac{1}{2}}. \tag{11}$$

The Kauffman number permits the incorporation of drop and cantilever length scales and liquid properties. We have arranged Ka such that increasing terms in the numerator promotes drop deformation by increasing drop volume and inertia and cantilever motion. Increasing the denominator magnitude reduces deformation by stiffening both solid and liquid. The drop placement distance from the tip $\ell - x_0$ is not included as a parameter, as it is fixed in our experiments, but is implicitly manifested in f, as is material stiffness. Cantilever width w, another fixed variable, is likewise excluded in Ka. Modification of Ka by a factor of $(\ell - x_0/w)$ could be included should drop location and w become variablized. Damping capacity ψ is plotted against Ka in Fig. 7(b). For each cantilever, Ka of $O(10^2)$ values permit the greatest damping, corresponding to moderately viscous fluids. In practice, to maximize damping of a given cantilever, one could select a liquid (ρ, μ) and drop size (R) to achieve a Ka of the desired value. During fluid selection, the damped natural frequency imposed by a given liquid is unknown, but for $m_d/m_c \approx 1-6$, the ratio $f/f_0 \approx 0.8-1$ where $f_0 = 0.56(EI/m_c\ell^3)^{1/2}$ is the cantilever's damped natural frequency in first mode vibration without added mass. Thus, either a calculated or observed f_0 provides a convenient substitute for f when calculating an approximate Ka. We plot (f/f_0) in Fig. 9(b).

V. DISCUSSION AND CONCLUDING REMARKS

In this study, we have experimentally determined the damping capacity of liquid drops resting on the free end of a vibrating cantilever. Our work may be compared to that of PIDs on cantilevers, which like drops, show decreased damping capacity at high levels of effective acceleration,[12] typically in the range of $\psi \approx 0.1-0.2$. At the effective accelerations in which PIDs work best, $\psi \approx 0.8-1$ However, at effective accelerations $\Gamma < 2$, the damping capacity of particle dampers falls dramatically, presumably due to the cessation of movement of particles within the damper. No such decline in damping capacity is witnessed with liquid drops, which can experience internal flow with the slightest of external excitation. Thus a functional comparison can be drawn between the two types of dampers. Liquid drop dampers may be suitable for applications where damping is needed at small perturbation amplitudes or small surface accelerations, whereas PIDs, not prone to break apart or eject, are more robust to failure at larger surface accelerations. A direct comparison between drops and PIDs is difficult because the measure of ψ is tied to cantilever inertia, air damping, and internal damping in addition to damper properties. For example, our 2.2-mg, 2-mil cantilever topped with a solid mass has a greater damping capacity than some of the 38-g cantilevers topped with PIDs simulated by Mao *et al.*[12]

The initial pluck amplitude of our system was chosen to ensure that drops never eject from our cantilevers. If ejection were no concern, we expect that specific damping would change very little up to the point where drops fail in cohesion and break apart. The curves of Figs. 6(a)–6(c) indicate that all test fluids approach a limit of ψ. The values of ψ for the 10-mil cantilever at $\Gamma = 400$ gravities are comparable to those at $\Gamma = 100$ gravities. The same behavior is seen with the other cantilevers, though at smaller effective acceleration ranges.

While wetting properties of the cantilever were held constant in our system, wettability is another means to tune drop damping. Hydrophobicity produces static drops which are more spherical, promotes contact line motion, and makes drops susceptible to ejection from the surface.[38,43] Drop motion across the substrate is likely unfavorable because it is difficult to control. Hydrophilic surfaces, in contrast, will produce flattened static drops, encourage contact line pinning, and permit higher accelerations before drops leave the surface. We posit, based on our results in Sec. IV A, the limited ability of flattened drops to undergo large deformation limits their ability to damp. Furthermore, pinned drops are not able to dissipate energy through contact line motion. Though we implicitly include dissipation by contact line friction, we are not able to separate it from viscous dissipation. Previous work[52,53] has discovered a closed form expression of a contact line friction coefficient,

$$\zeta = \frac{\mu V_m}{\lambda^3}\exp\frac{\sigma\lambda^2(1+\cos\theta_c)}{k_b T}, \tag{12}$$

where V_m is the molecular volume of the unit of flow, k_B is the Boltzmann constant, and T is the absolute temperature. There "no way of definitively predicting" the molecular jump distance λ from one potential well to another for a given solid–liquid combination.[52] However, Eq. (12) is illuminating in terms of how dissipation via friction scales with viscosity and surface tension. The identification of λ and V_m for a given system is a step toward optimizing liquid properties, μ and σ, to maximize damping.

The damping of the cantilever by a drop will be strongly correlated with the ratio of the cantilever to drop mass. Cantilevers of different density or thickness to the ones tested innately have different

natural frequencies, which in turn modulates drop deformation, i.e., flatness factor, as shown in Figs. 6(d)–6(f). Our most massive 10-mil cantilever has a cantilever-drop mass ratio of approximately six and experiences less damping than the 5-mil specimen with a mass ratio of three. For 2-mil thick cantilevers, the drop mass is roughly equivalent to the cantilever mass, sloshing drop can alter the cantilever phase, revealing two dominant frequencies as reported in Figs. 4(a) and 4(b). The emergence of two frequencies is perhaps the cause for less damping in the 2-mil cantilever than one might expect, but our physical understanding of this observation is limited.

The introduction of non-Newtonian fluids is another avenue for tuning the damping characteristics of drops but will dramatically increase the difficulty in predicting system behavior. The shear-stress dependency of non-Newtonian fluid properties dictates that damping capacity will be highly reliant on cantilever accelerations. At large accelerations, shear-thickening fluids will behave more solid, and perhaps see a dramatic reduction in damping capacity. Shear-thinning fluids could be prone to erratic breakup. The emergence of such behaviors is of course be governed by the matching of the solid and liquid composition.

We hope our results form a foundation for engineered systems to both use liquid damping, in the case of novel sensors, and thwart it, in the case of robotic flyers. The success of micro and nano aerial vehicles in all environments is critically dependent on their ability to cope with environmental hazards such as rainfall dewfall. The removal of moisture from flight critical surfaces may not be trivial for the smallest flyers.[56,57] Vibration strategies specifically employed to dry wings much be chosen to maximize efficacy by minimizing input. A critical piece to effective self-drying is an understanding of vibration damping by the very mass a flyer seeks to remove.

SUPPLEMENTARY MATERIAL

See the supplementary material for an additional plot of temporal displacement curves of the 2-mil cantilever topped by various drops.

ACKNOWLEDGMENTS

We would like to thank Tianyi Li for assistance with viscosity and surface tension measurements and Michael Cassette for his experimental and data analysis contributions.

We would like to thank the NSF CBET-1941341 for support.

DATA AVAILABILITY

The data that support the findings of this study are openly available in perpetuity via Open Science Framework at https://osf.io/pjnqh/, Ref. 58.

REFERENCES

[1]M. Kimber, R. Lonergan, and S. Garimella, "Experimental study of aerodynamic damping in arrays of vibrating cantilevers," J. Fluids Struct. **25**, 1334–1347 (2009).
[2]R. A. Bidkar, M. Kimber, A. Raman, A. K. Bajaj, and S. V. Garimella, "Nonlinear aerodynamic damping of sharp-edged flexible beams oscillating at low Keulegan–Carpenter numbers," J. Fluid Mech. **634**, 269–289 (2009).
[3]V. Valamanesh and A. Myers, "Aerodynamic damping and seismic response of horizontal axis wind turbine towers," J. Struct. Eng. **140**, 04014090 (2014).
[4]J. Yang, T. Ono, and M. Esashi, "Energy dissipation in submicrometer thick single-crystal silicon cantilevers," J. Microelectromech. Syst. **11**, 775–783 (2002).
[5]H. Hosaka, K. Itao, and S. Kuroda, "Evaluation of energy dissipation mechanisms in vibrational microactuators," in *Proceedings IEEE Micro Electro Mechanical Systems an Investigation of Micro Structures, Sensors, Actuators, Machines and Robotic Systems* (IEEE, 1994), pp. 193–198.
[6]K. Y. Yasumura, T. D. Stowe, E. M. Chow, T. Pfafman, T. W. Kenny, B. C. Stipe, and D. Rugar, "Quality factors in micron-and submicron-thick cantilevers," J. Microelectromech. Syst. **9**, 117–125 (2000).
[7]W. E. Baker, W. E. Woolam, and D. Young, "Air and internal damping of thin cantilever beams," Int. J. Mech. Sci. **9**, 743–766 (1967).
[8]A. Papalou and S. Masri, "Response of impact dampers with granular materials under random excitation," Earthquake Eng. Struct. Dyn. **25**, 253–267 (1996).
[9]Z. Xu, M. Y. Wang, and T. Chen, "Particle damping for passive vibration suppression: Numerical modelling and experimental investigation," J. Sound Vib. **279**, 1097–1120 (2005).
[10]R. D. Friend and V. K. Kinra, "Particle impact damping," J. Sound Vib. **233**, 93–118 (2000).
[11]M. Duncan, C. Wassgren, and C. Krousgrill, "The damping performance of a single particle impact damper," J. Sound Vib. **286**, 123–144 (2005).
[12]K. Mao, M. Y. Wang, Z. Xu, and T. Chen, "Simulation and characterization of particle damping in transient vibrations," J. Vib. Acoust. **126**, 202–211 (2004).
[13]S. E. Olson, "An analytical particle damping model," J. Sound Vib. **264**, 1155–1166 (2003).
[14]Z. Lu, Z. Wang, S. F. Masri, and X. Lu, "Particle impact dampers: Past, present, and future," Struct. Control Health Monit. **25**, e2058 (2018).
[15]M. Saeki, "Impact damping with granular materials in a horizontally vibrating system," J. Sound Vib. **251**, 153–161 (2002).
[16]C. Wong, M. Daniel, and J. Rongong, "Energy dissipation prediction of particle dampers," J. Sound Vib. **319**, 91–118 (2009).
[17]G. Michon, A. Almajid, and G. Aridon, "Soft hollow particle damping identification in honeycomb structures," J. Sound Vib. **332**, 536–544 (2013).
[18]L. Kempton, D. Pinson, S. Chew, P. Zulli, and A. Yu, "Simulation of macroscopic deformation using a sub-particle dem approach," Powder Technol. **223**, 19–26 (2012).
[19]S. Ashley, "A new racket shakes up tennis," Mech. Eng.-CIME **117**, 80–82 (1995).
[20]H. Panossian, "Structural damping enhancement via non-obstructive particle damping technique," J. Vib. Acoust. **114**, 101–105 (1992).
[21]R. Ehrgott, H. Panossian, and G. Davis, "Modeling techniques for evaluating the effectiveness of particle damping in turbomachinery," in 50th AIAA/ASME/ASCE/AHS/ASC Structures, Structural Dynamics, and Materials Conference (2009), p. 2690.
[22]S. S. Simonian, "Particle beam damper," in *Smart Structures and Materials 1995: Passive Damping* (International Society for Optics and Photonics, 1995), Vol. 2445, pp. 149–160.
[23]H. Akyildiz and E. Ünal, "Experimental investigation of pressure distribution on a rectangular tank due to the liquid sloshing," Ocean Eng. **32**, 1503–1516 (2005).
[24]M. Eswaran and U. K. Saha, "Sloshing of liquids in partially filled tanks–a review of experimental investigations," Ocean Syst. Eng. **1**, 131–155 (2011).
[25]E. L. Grotle and V. Æsøy, "Numerical simulations of sloshing and the thermodynamic response due to mixing," Energies **10**, 1338 (2017).
[26]H. Luskin and E. Lapin, "An analytical approach to the fuel sloshing and buffeting problems of aircraft," J. Aeronaut. Sci. **19**, 217–228 (1952).
[27]P. Caron, M. Cruchaga, and A. Larreteguy, "Study of 3D sloshing in a vertical cylindrical tank," Phys. Fluids **30**, 082112 (2018).
[28]S. aus der Wiesche, "Noise due to sloshing within automotive fuel tanks," Forsch. Ingenieurwes. **70**, 13–24 (2005).
[29]R. He, E. Zhang, and B. Fan, "Numerical analysis on the sloshing of free oil liquid surface under the variable conditions of vehicle," Adv. Mech. Eng. **11**, 1–13 (2019).
[30]E. Frosina, A. Senatore, A. Andreozzi, F. Fortunato, and P. Giliberti, "Experimental and numerical analyses of the sloshing in a fuel tank," Energies **11**, 682 (2018).
[31]O. Faltinsen, R. Firoozkoohi, and A. Timokha, "Analytical modeling of liquid sloshing in a two-dimensional rectangular tank with a slat screen," J. Eng. Math. **70**, 93–109 (2011).
[32]P. Behruzi, M. Konopka, F. de Rose, G. Schwartz *et al.*, "Cryogenic slosh modeling in LNG ship tanks and spacecrafts," in *The Twenty-Fourth*

International Ocean and Solar Engineering Conference (International Society of Offshore and Polar Engineers, 2014).
[33]R. A. Ibrahim, *Liquid Sloshing Dynamics: Theory and Applications* (Cambridge University Press, 2005).
[34]F. Welt and V. Modi, "Vibration damping through liquid sloshing, Part 2: Experimental results," ASME J. Vib. Acoust. **114**(1), 17–23 (1992).
[35]A. Sauret, F. Boulogne, J. Cappello, E. Dressaire, and H. A. Stone, "Damping of liquid sloshing by foams," Phys. Fluids **27**, 022103 (2015).
[36]D. Kannangara, H. Zhang, and W. Shen, "Liquid–paper interactions during liquid drop impact and recoil on paper surfaces," Colloids Surf., A **280**, 203–215 (2006).
[37]X. Yang, V. H. Chhasatia, and Y. Sun, "Oscillation and recoil of single and consecutively printed droplets," Langmuir **29**, 2185–2192 (2013).
[38]M. E. Alam, J. L. Kauffman, and A. K. Dickerson, "Drop ejection from vibrating damped, dampened wings," Soft Matter **16**, 1931–1940 (2020).
[39]X. Tang, A. Saha, C. Sun, and C. K. Law, "Spreading and oscillation dynamics of drop impacting liquid film," J. Fluid Mech. **881**, 859–871 (2019).
[40]J. Zheng, Y. Cheng, Y. Huang, S. Wang, L. Liu, and G. Chen, "Drop impacting on a surface with adjustable wettability based on the dielectrowetting effect," Phys. Fluids **32**, 097108 (2020).
[41]A. James, B. Vukasinovic, M. K. Smith, and A. Glezer, "Vibration-induced drop atomization and bursting," J. Fluid Mech. **476**, 1–28 (2003).
[42]R. M. Manglik, M. A. Jog, S. K. Gande, and V. Ravi, "Damped harmonic system modeling of post-impact drop-spread dynamics on a hydrophobic surface," Phys. Fluids **25**, 082112 (2013).
[43]M. E. Alam, D. Wu, and A. K. Dickerson, "Predictive modelling of drop ejection from damped, dampened wings by machine learning," Proc. R. Soc. A **476**, 20200467 (2020).
[44]M. Oroian, "Measurement, prediction and correlation of density, viscosity, surface tension and ultrasonic velocity of different honey types at different temperatures," J. Food Eng. **119**, 167–172 (2013).
[45]P. A. Gorry, "General least-squares smoothing and differentiation by the convolution (Savitzky-Golay) method," Anal. Chem. **62**, 570–573 (1990).
[46]D. A. Watson, J. L. Stephen, and A. K. Dickerson, "Impacts of free-falling spheres on a deep liquid pool with altered fluid and impactor surface conditions," J. Visualized Exp. **144**, e59300 (2019).
[47]D. A. Watson, C. J. Souchik, M. P. Weinberg, J. M. Bom, and A. K. Dickerson, "Making a splash with fabrics in hydrophilic sphere entry," J. Fluids Struct. **94**, 102907 (2020).
[48]N. M. Smith, G. V. Clayton, H. A. Khan, and A. K. Dickerson, "Mosquitoes modulate leg dynamics at takeoff to accommodate surface roughness," Bioinspiration Biomimetics **14**, 016007 (2018).
[49]N. M. Smith, J. B. Balsalobre, M. Doshi, B. J. Willenberg, and A. K. Dickerson, "Landing mosquitoes bounce when engaging a substrate," Sci. Rep. **10**, 1–10 (2020).
[50]M. Pasandideh-Fard, Y. Qiao, S. Chandra, and J. Mostaghimi, "Capillary effects during droplet impact on a solid surface," Phys. Fluids **8**, 650–659 (1996).
[51]A. K. Dickerson, P. G. Shankles, and D. L. Hu, "Raindrops push and splash flying insects," Phys. Fluids **26**, 027104 (2014).
[52]T. D. Blake, "The physics of moving wetting lines," J. Colloid Interface Sci. **299**, 1–13 (2006).
[53]M. Voué, R. Rioboo, M. Adao, J. Conti, A. Bondar, D. A. Ivanov, T. D. Blake, and J. De Coninck, "Contact-line friction of liquid drops on self-assembled monolayers: Chain-length effects," Langmuir **23**, 4695–4699 (2007).
[54]D. Zang, W. Zhang, J. Song, Z. Chen, Y. Zhang, X. Geng, and F. Chen, "Rejuvenated bouncing of non-newtonian droplet via nanoparticle enwrapping," Appl. Phys. Lett. **105**, 231603 (2014).
[55]C. Loudon and A. Tordesillas, "The use of the dimensionless womersley number to characterize the unsteady nature of internal flow," J. Theor. Biol. **191**, 63–78 (1998).
[56]A. K. Dickerson and D. L. Hu, "Mosquitoes actively remove drops deposited by fog and dew," Integr. Comp. Biol. **54**, 1008–1013 (2014).
[57]A. K. Dickerson, X. Liu, T. Zhu, and D. L. Hu, "Fog spontaneously folds mosquito wings," Phys. Fluids **27**, 021901 (2015).
[58]A. K.Dickerson, "Sessile drops damp vibrating substrates," Open Science Framework. https://osf.io/pjnqh/